The preparation of core-shell-like zeolite by diffusion controlled chemical etching

Yanfeng Shen, Mingrui Xu, Jingyang Li, Zhengxing Qin, Chunzheng Wang, Svetlana Mintova, Xinmei Liu

The preparation of core-shell-like zeolite by diffusion controlled chemical etching

Yanfeng Shen,[a] Mingrui Xu,[a] jingyang Li,[a] Zhengxing Qin,[*a] Chunzheng Wang,[a] Svetlana Mintova,[a,b] and Xinmei Liu[*a]

The present work reports on the preparation of core-shell-like zeolites with Si-rich mesoporous shell. This is achieved by diffusion controlled chemical etching of zeolite crystals with a mixture containing oxalic acid and ammonium fluoride (OA-NH_4F). The OA-NH_4F served as a bifunctional etchant extracting both surface Si and Al and further dealuminating the periphery of the zeolite crystals. The fast dissolution kinetics and the relatively slow intra-crystalline diffusion of the OA-NH_4F etching solutions resulted in a distinct core-shell-like structure with porous and Si-rich shell keeping the unique advantages of single crystals with interconnected micro- and mesopores.

Introduction

Zeolites, crystalline microporous aluminosilicates, are widely used in industrial processes as shape-selective catalysts thanks to their well-defined structure, variable chemical composition and surface acidity and outstanding thermal and hydrothermal stability [1, 2]. The sub-nanometer sized micropores are the unique advantage of zeolites for shape-selective catalysis. On the other hand, however, for reactions involving bulky molecules with size greater than zeolite micropores, the intra-particle diffusion of reactants and intermediate products in and out zeolite crystals become an important concern for zeolites scientists. To address this mass transport issue, several characteristic approaches have been developed, which including nano zeolites [3], extra-large micropore zeolites [4], and hierarchical zeolites [5]. As the most versatile method for improving the intra-particle diffusion efficiency of existing zeolites, hierarchization has been developed as the most popular treatment for the post-synthetic engineering of zeolite that are prepared in large scale at industrial level [6].

During the preparation of hierarchical zeolites, the persistence of crystal surface

is commonly observed but often ignored [7-11]. This surface of zeolite crystals is characterized by the universal formation of a "crust" on the outermost layer, no matter the post synthesis treatment including desilication-biased caustic leaching [12-16], dealumination-biased acidic treatment [7-9], or Si and Al unbiased NH_4F etching [11]. Typically, the formation of such a crust was attributed to an Al-zoning induced inhomogeneous dissolution of zeolite crystals [17]. This is originated from the interpretation that the preferential sitting of Al on zeolite rim protects the outermost shell from dissolution. The preferential dissolution of Si-rich core collaboratively leads to the formation of hollow zeolite structure. Alternatively, the difficulty to engineer the outermost shell of zeolite crystals is related to its less defective nature [11]. The "coat" is formed at the very end of a zeolite crystallization process [18-21]. While at this step, the crystallization medium shapes the final surface of zeolites, it also creates a less-defective outermost shell resistive to chemical treatments [11, 22]. The surface resistance of zeolites to chemical etching has not been decisively studied. We anticipate that the transformation of the outermost layer of zeolites to a highly porous shell can be highly favorable for the adsorption of bulky molecules.

The research interest in engineering of zeolite surface is further stimulated by the recent results showing that transport of molecules through microporous crystals can be significantly influenced by diffusion [23, 24]. The crystal periphery is the first path the molecules encounter during the diffusion into zeolite crystals. To alleviate the surface barriers, post-synthetic modification of the zeolite surface was conducted. In this respect, the covering of a mesoporous and inert over-layer on top of zeolite surface has been proven successful in enhancing the sorption rate because of an increased sticking probability [25]. The preparation of zeolitic core-shell materials with zeolite core and mesoporous shell was reported [26-31]. The preparation of core-shell zeolite composites with an integral core and shell parts free of interface boundary are rare. The engineering of zeolite crystals with core-shell structures consisting of a rough mesoporous shell and a zeolitic core would be interesting due to the simultaneous enhancement of surface diffusion and the large preservation of the

intrinsic zeolite properties.

In recent years, we focused on the fluoride etching approach (see Figure 1 below) towards post-synthetic engineering of zeolites crystals. The uniqueness in the preparation of mesoporous zeolites with intact microporosity and acidity was demonstrated [32]. Additionally, we revealed the formation of extended intergrown subunits in zeolite crystals with MFI type structure [33], the uncovering of the inner mosaic structure of zeolite crystals [32], the opening of previously inaccessible zeolite cages [34] and side pockets [35]. The inner heterogeneity of ZSM-5 zeolite crystals was recently revealed by our group [22]. The studies above were performed taking the unique advantage of fluoride etching approach (NH_4F etching, "III" in Figure R1) leading to unbiased removal of Si and Al from the zeolite framework. This sharply contrasts the Si-biased dissolution of zeolite crystals in alkaline media, and the Al-biased dealumination by steaming and/or acid leaching.

Herein, we report a new etchant for the "top-down" preparation of a core-shell-like hierarchical zeolite. Zeolite Y (FAU type framework structure), the most commercially used zeolite in heterogeneous catalysis was prepared as a core-shell-like hierarchical material comprised of a rough mesoporous shell and a microporous core, both of which possess the same cohesive zeolite structure.

Experimental

2.1 Preparation of single core-shell-like zeolite crystals

Commercial zeolite Y (LZY-62 from UOP, Si/Al = 2.6) was used in this study. Before chemical etching, the starting material was ion-exchanged three times with a 1 mol/L aqueous ammonium chloride (99.5%, Sinopharm Chemical Reagent Corporation) solution at liquid/solid ratio of 20. The ammonium exchange was carried out at 363 K for 3 h each time. The sample was thoroughly washed using deionized water after each ion exchange. The resulting zeolite was used as the parent sample (PY) for the subsequent treatments.

The acidic etching of PY with oxalic acid was performed as follow: 5 g PY and 5

g ammonium sulfate (99.0%, Sinopharm Chemical Reagent Corporation) were dispersed in 50 g deionized water under stirring at room temperature. Then 17.5 g of 1 mol/l oxalic acid (99.5%, Sinopharm Chemical Reagent Corporation) solution was added dropwise into the zeolite suspension within 20 min. The acid treatment was conducted for 2 h under stirring at room temperature. After that, the acid treated product was recovered by vacuum filtration, washed thoroughly with deionized water and dried at 373 K overnight. The resulting sample was denoted as AY.

The other sample abbreviated as FY was prepared by treating the parent zeolite (PY) with NH_4F solution. 5 g PY and 5 g ammonium sulfate (99.0%, Sinopharm Chemical Reagent Corporation) were dispersed into 50 g deionized water. 5 g NH_4F was then added into the mixture under magnetic stirring. The process was kept at room temperature for 2 h. The product was separated by filtration, washed with deionized water thoroughly and dried under 373 K overnight.

The treatment of sample PY with oxalic acid-ammonium fluoride (OA-NH_4F) was carried as follows: 5 g of PY and 5 g ammonium sulfate was dispersed in 50 g deionized water under stirring at room temperature. Then an oxalic acid-ammonium fluoride mixture made of 5 g ammonium fluoride and 17.5 g or 10 g 1M oxalic acid solution, was added. The obtained suspension was kept at room temperature for 2 h under stirring. After that, the products were recovered by vacuum filtration, washed thoroughly with water and dried at 373 K overnight. The sample treated by OA-NH_4F with a higher (17.5 g) or lower (10 g) concentration of oxalic acid were denoted as AFY1 and AFY2 respectively.

2.2 Characterization

X-ray diffraction measurements were performed on an X`pert Pro/PANalytical Diffractometer using Cu Kα radiation (λ = 1.5418 Å, 45 kV, 40 mA). The samples were studied in the 5-50° 2θ range with a scanning step of 0.0167° s^{-1}.

Electron micrographs were taken on a JSM-7900F (JEOL) low-voltage high-resolution scanning electron microscope (SEM) equipped with a field emission

gun. The cross-section of the AFY1 and AFY2 zeolites were obtained by using an ion Beam cross-section polisher (IB-19510CP, JEOL). Transmission electron microscopy (TEM) images were recorded using a JEOL 2100F microscope at 200 kV.

Nitrogen adsorption/desorption isotherms were recorded with a Micromeritics ASAP 2020 automated gas adsorption analyzer. Prior to analysis, the samples were out gassed at 373 K for 1 h and 573 K for 10 h. Specific surface areas were determined from the BET equation applied to the 0.01 - 0.06 p/p^0 range. The total pore volume was taken from nitrogen adsorbed volume at p/p^0 = 0.97. The t-plot method, applied in the 0.4 - 0.8 range, was used to distinguish the micropores from the mesopores in the samples.

^{27}Al MAS NMR spectra were recorded on a Bruker Advance 500 MHz spectrometer using a 4 mm rotor. The ^{27}Al MAS NMR spectra were recorded at 104.3 MHz with a 12 pulse length of 2.2 μs, a spinning rate of 14 kHz and a recycle delay of 1 s. 1 M $Al(NO_3)_3$ was used as reference for chemical shifts of ^{27}Al.

Infrared spectra were recorded using a Nicolet Magna 550-FT-IR spectrometer with 2 cm^{-1} optical resolution. Prior to the measurements, the samples were pressed into self-supporting discs (diameter: 1.6 cm, ~17 mg) and preheated in the IR cell attached to a vacuum line at 723 K (2 K /min) for 5 h down to 10^{-6} Torr. The adsorption of pyridine was performed at 373 K. After establishing a pressure of 1 Torr at equilibrium, the cell was then evacuated at 423 - 673 K and the amount of pyridine remaining adsorbed on Brønsted and Lewis sites determined using the integrated area of the bands observed at 1545 cm^{-1} and 1454 cm^{-1}, respectively. All spectra were normalized to 20 mg wafers. The extinction coefficients used were $\varepsilon(B)_{1545} = 1.3$ and $\varepsilon(L)_{1455} = 1.5$. The desorption temperature selected for the quantitative measurement of acidity by pyridine was 473 K.

The chemical composition of parent and treated samples was measured by XRF. The surface component of zeolites was probed by X-ray photoelectron spectroscopy (XPS) with a PHI 500 spectrometer using Al Ka radiation.

2.3 Catalytic test

The conversion of 1,3,5-triisopropylbenzene (TiPBz) was performed in a tubular flow reactor operating in gas phase at atmospheric pressure (1×10^5 Pa). For each experiment, 20 mg of zeolite were loaded in the reactor enclosed between two layers of inert SiC (200 ~ 400 μm size range). The samples were carefully activated in a dry-air stream (50 $mL\cdot min^{-1}$), first at 373 K for 1 h, and then the temperature raised to 450 °C (ramp of 1.5 $°C\cdot min^{-1}$) and maintained 3 h at this temperature. N_2 was subsequently introduced and the reactor cooled-down to the reaction temperature (498 K). A stream of 200 $mL\cdot min^{-1}$ N_2 was diverted to a saturator filled with TiPBz maintained at 72 °C (P_{TiPBz} = 192 Pa). A unique space time, W/F_0, of 0.022 $kg\cdot h\cdot mol^{-1}$ was used. Stable conditions were established in less than 5 minutes; the products were analyzed after 5 min, thereafter at 15 min intervals on a CPG (VARIAN Cp 3800; HP-Pona 50 m, 0.2 mm, 0.5 μm column) with a FID detector.

3. Results and discussion

3.1 Dynamic chemical equilibrium in aqueous oxalic acid-NH_4F medium

In order to transfer the tough zeolite "coat" into a porous shell, an intensive dissolution of the surface zeolite layer is a prerequisite. Therefore, a highly reactive etchant that is both active for Si and Al removal was applied. The aqueous oxalic acid-NH_4F mixture (OA-NH_4F) was used. This is based on our previous finding that NH_4F-HF mixed solution is able to extract both framework Si and Al unbiasedly [33]. The co-presence of F^- and HF shifts the chemical equilibria and produce in-situ the active fluoride species such as HF, H_2F_2, HF_2^- that are active for Si and Al removal [32]. Oxalic acid was used here to avoid the direct use of hazardous HF. The higher acid dissociation constant of oxalic acid ($K_{a1} = 5.9 \times 10^{-2}$) suppresses the dissociation of HF ($K_a = 6.8 \times 10^{-4}$) into H^+ and F^- (① and ② in Scheme 1), thus favoring the equilibrium loop towards HF, H_2F_2 and HF_2^- formation (④, ⑤ and ⑥ in Scheme 1). What is of additional interest is the chelating properties of oxalic acid [36, 37]. As will

discussed later, the presence of chelating agent has added a new and interesting variable (dealumination) to the chemical etching of zeolite in fluoride medium.

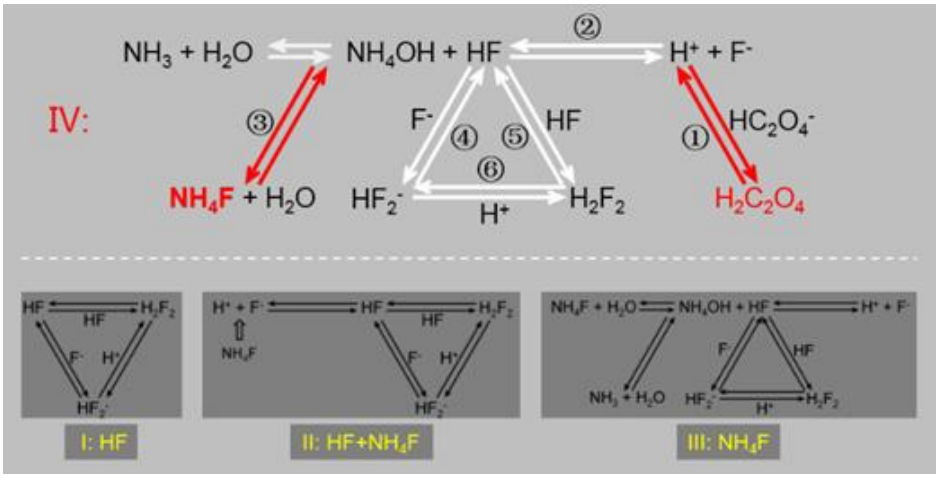

Scheme 1. (I – IV) The evolution of the fluoride etching toolkit for the post-synthetic engineering of zeolite crystals. (IV) The hydrolysis of oxalic acid (①) and fluoride species (② – ⑥) in aqueous oxalic acid and NH_4F mixture.

3.2 Characterization of core-shell-like zeolites

The addition of OA-NH_4F into the zeolite suspension (Experimental part) increased the pH immediately from 5.5 to above 7, then it continued to increase slowly and stabilized at around 8 (Figure S1). This distinct increase in pH and the release of ammonia are obvious signs of the ongoing hydrolysis of NH_4F and progressive consumption of HF (②, ④, ⑤ and ⑥ in Scheme 1). Hence a progressive etching of zeolite crystals can be expected.

After the chemical treatment, the samples were characterized by XRD. The XRD patterns of the parent and treated zeolites are shown in Figure l. All samples show well-defined Bragg peaks characteristic of FAU-type zeolite, regardless of the crystallinity. These samples were subjected to nitrogen physisorption analysis. FY, the NH_4F etched zeolite Y, displays a typical type I isotherms similar to parent Y (PY).

The parent zeolite Y exhibits a higher adsorption capacity for nitrogen at lower relative pressure p/p^0 (Figure 2a, Table 1), which is characteristic of a highly crystalline microporous zeolite. The almost complete absence of mesoporosity for sample FY clearly indicates that the applied NH_4F etching alone did not lead to the considerable dissolution of the parent zeolite crystals. This is because the concentration of NH_4F used in the present work is much lower than the one reported before [34]. On the other side, the chemical treatment with pure oxalic acid resulted in a sample (AY) with a marked low microporosity (Figure 2a and Table 1), which is in agreement with the XRD (Figure 1). However, the loss of microporosity did not lead to an increase in mesoporosity (Table 1). In contrast, the AFY1 sample treated by oxalic acid – NH_4F mixed solution, shows high adsorption of nitrogen at lower p/p^0 (Figure 2a). The micropore volume of AFY1 is 0.22 cm^3g^{-1} (Table 1). In addition, the N_2 adsorption isotherm exhibits a continuous uptake between ca. 0.01 and 0.8 p/p^0 and a hysteresis loop at p/p^0 of ca. 0.4 (Figure 2a). This result indicates that there are small mesopores or even large secondary micropores formed in the AFY1 zeolite crystals [38]. The pore size distribution (PSD) curves calculated from both the adsorption and desorption branches of the isotherms show noticeable peaks in 2 - 10 nm range (Figure 2b, c). Thus, the XRD and N_2 physisorption results provide the first sign that pure NH_4F, pure oxalic acid and their mixture etched differently the zeolite crystals.

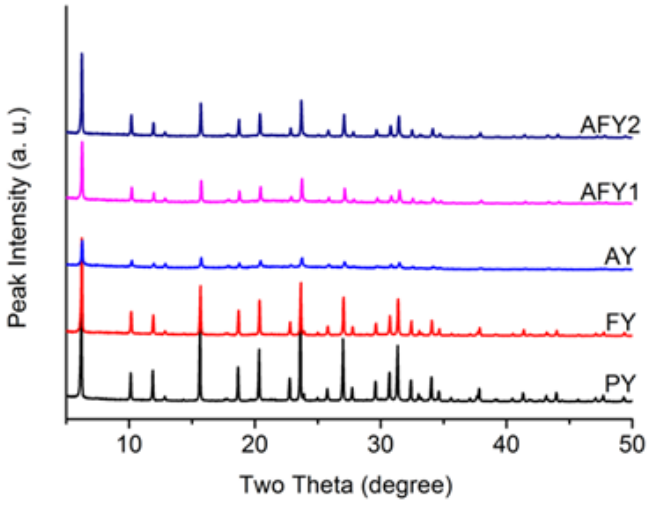

Figure 1. XRD patterns of the parent Y zeolite (PY) and its derivatives prepared by chemical etching using NH_4F (FY), oxalic acid (AY) and oxalic acid – NH_4F mixture (AFY1, 2).

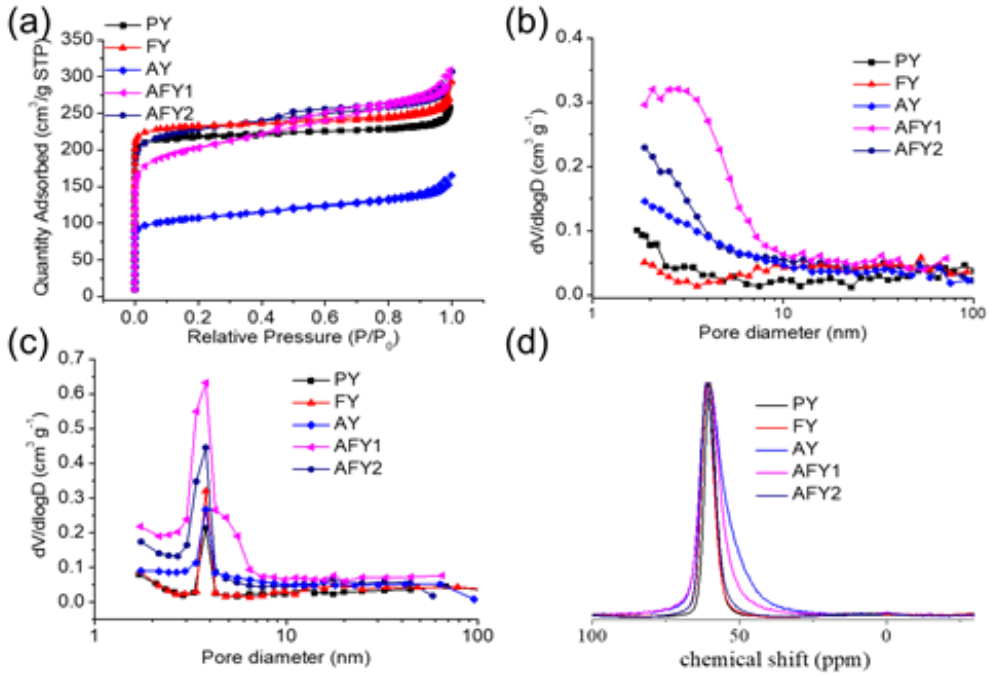

Figure 2. N_2 sorption isotherms (a), BJH pore size distribution (b: adsorption, c: desorption) and ^{27}Al NMR spectra (d) of the parent Y, NH_4F (FY), oxalic acid (AY) and OA-NH_4F mixed solution (AFY1 and AFY2) treated zeolites.

Table 1. Physicochemical characteristics of the series of zeolite Y samples subjected to chemical etching.

samples	Si/Al[a]	S_{BET}[b]	S_{ext}[c]	V_{mic}[c]	V_{meso}[d]	B_{Py}[e]	L_{Py}[e]
		$m^2 \cdot g^{-1}$	$m^2 \cdot g^{-1}$	$m^3 \cdot g^{-1}$	$m^3 \cdot g^{-1}$	$\mu mol \cdot g^{-1}$	$\mu mol \cdot g^{-1}$
PY	2.6	697	16	0.34	0.04	1069	96
FY	2.7	741	22	0.35	0.07	1003	53
AY	5.4	352	92	0.13	0.10	299	239

AFY1	5.5	671	210	0.22	0.22	544	86
AFY2	4.0	740	133	0.30	0.14	731	143

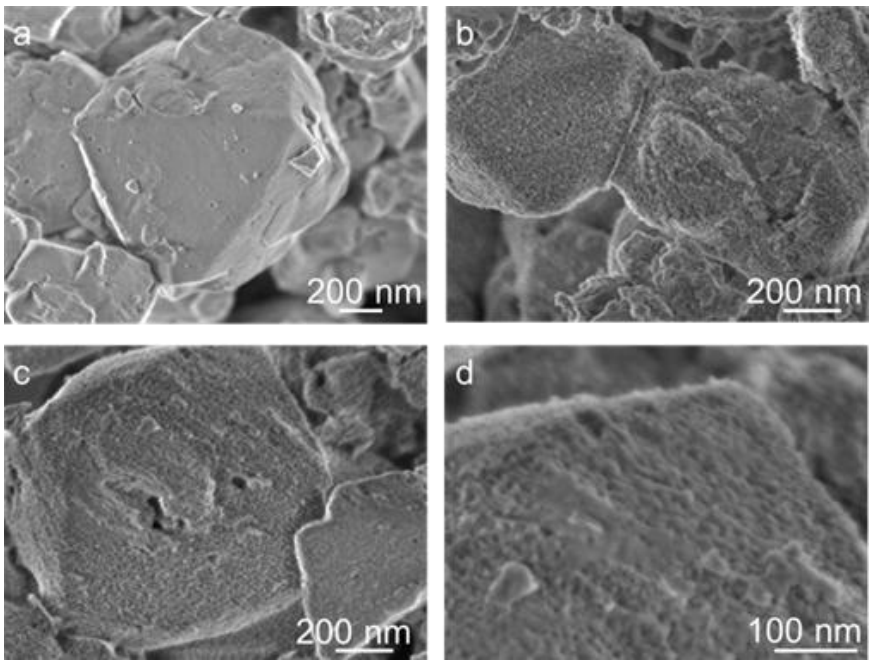

Figure 3. SEM images of the parent zeolite Y sample (a) and sample AFY1 after treatment with OA-NH4F solution at different magnifications (b-d).

The parent and treated zeolites were further studied by SEM, TEM and SEM-EDX mapping. High resolution low voltage SEM show unambiguously that the etching by OA-NH_4F leads to a remarkably roughened external surface in the case of AFY-1 zeolite sample (Figure 3b-d). Such a rough surface sharply contrasts the smooth feature of the parent sample (PY, Figure 3a) and the one treated by oxalic acid (AY, Figure S3a) or NH_4F (FY, Figure S3b). Noting that both AY and FY were prepared by chemical etching of PY with the same amount of oxalic acid and NH_4F as that for AFY1 (see experimental section). In addition, the surface of AFY1 looks also different from that of ultra-stable Y [39] and surfactant-templated mesostructured Y zeolites [40].

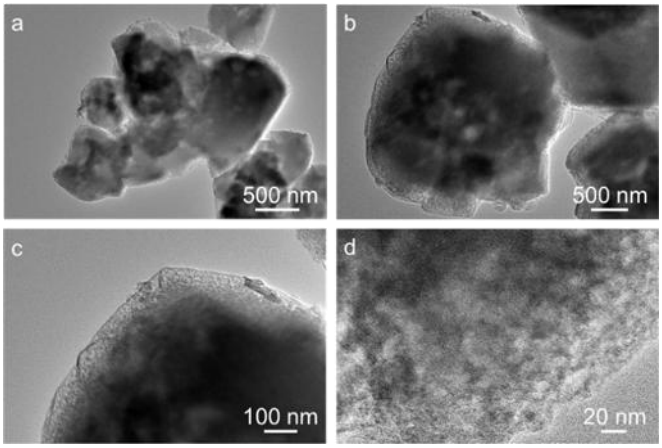

Figure 4. TEM images of the AFY1 zeolite crystals at different magnifications (a-d).

In contrast to the homogeneous and dense PY zeolite crystals seen by TEM (Figure S4)**,** the AFY1 shows a distinct core-shell-like structure with a highly porous shell (Figure 4). The porous shell has a thickness of about 100 nm. No dense outermost crust similar to those reported in previous studies was observed [7, 41]. Compared with the classical core-shell materials [31, 42], a clear-cut separation between the core and the shell was not observed in the present work. The hierarchical shell part increases its density progressively from the periphery to the central part of zeolite crystals. High resolution TEM reveals the presence of lattice fringes near the exterior of the particles (Figure S5), suggesting the partial preservation of the crystalline zeolite Y.

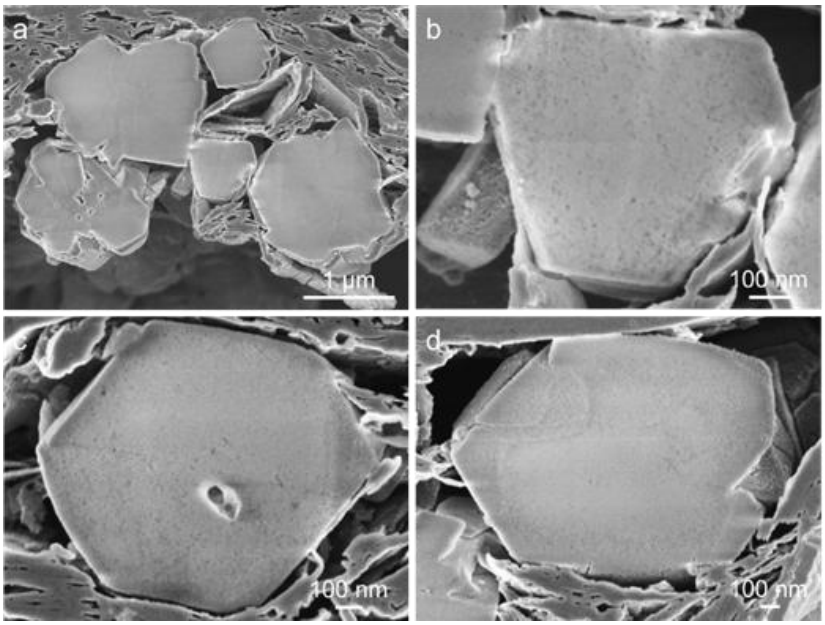

Figure 5. Cross-section SEM images of different AFY1 zeolite crystals (a-d).

In order to get more comprehensive information about the internal structural characteristics of the core-shell-like zeolite, AFY1 was cut with an ion beam cross-section polisher and the SEM images are depicted in Figure 5. As shown, most mesopores are distributed in the periphery of the cut crystals no matter the size of the zeolite crystals, while the inner part is less porous. In addition to the mesopores that can be distinguished under the applied conditions for SEM observation, there are many other small mesopores which are "invisible" due to the SEM resolution limit. The presence of small mesopores is indicated by the nitrogen physisorption results (Figure 2a, 2b). Whether they can be "seen" or not, the chemically induced mesopores all together contributed to the formation of a porous shell in the AFY1 zeolite. This mesopore-zoning is clearly indicated by the darker contrast of the crystal rim in the cross-section SEM images. Noting that the intensity of the generated secondary electrons varies depending on the density of the substance, i.e. darker contrast corresponds to less intense secondary electrons, hence to a less dense zone [11].

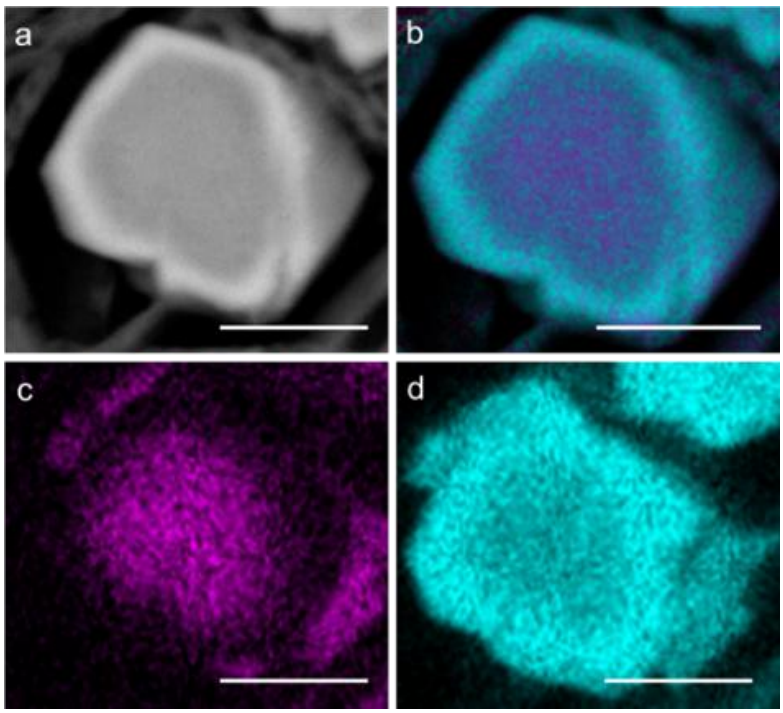

Figure 6. SEM and EDX mapping of AFY1 zeolite crystal (a: SEM image, b: EDX mapping image of overlapping Al with Si, c: EDX mapping image of Al, d: EDX

mapping image of Si, scale bar = 500 nm).

The distinct difference showing the core-shell-like characteristic of AFY1 zeolite is further provided by SEM-EDX mapping results (Figure 6), where a bright ring indicating a substantial Si-zoning in the crystal periphery is clearly distinguished. In contrast, the core part is richer in Al and the spatial distribution of Si and Al in this part is homogeneous. The bulk Si/Al ratio of 5.5 for the hierarchical core-shell-like zeolite is determined by XRF. While the surface Si/Al ratio of 14.3 for the same sample was determined by XPS analysis. These observations related with size and spatial distribution of mesopores and the thickness of the shell (~150 nm) of the zeolite crystals are in a good agreement with the TEM results (Figure 4).

The combined information from XRD, SEM, TEM and N_2 physisorption confirmed that a crystalline core-shell-like hierarchical zeolite with a rough mesoporous shell was prepared. This was achieved by chemical etching with OA-NH_4F solutions, which resulted in the extensive removal of Si and Al from the surface of zeolite crystals. The ^{27}Al MAS NMR spectrum of AFY1 shows a single peak at ca. 60 ppm highlighting the sole presence of tetrahedral aluminum (Figure 2d). The chemical etching leaded to a noticeable increase of Si/Al ratio in crystal periphery (shell); the substantial removal of both Si and Al from zeolite surface is presented in Figure 6. The Si and Al unbiased chemical etching characteristics for other fluorine-containing media was reported earlier [32, 33, 43]. The substantial dealumination behavior is most probably related to the high acid dissociation constant and chelating effect of the oxalic acid.

In agreement with the observed increase of the Si/Al ratio, the IR spectroscopy using pyridine as a probe molecule shows that the Brønsted acidity of sample OA-NH_4F dropped by half as compared with the parent zeolite (Table 1, Figure S6). The Brønsted acidity of AFY1 is much higher than that of the sample treated with oxalic acid (Table 1, Figure S6). Thus, the presence of NH_4F in the OA-NH_4F is not only crucial for the substantial removal of surface Si and Al leading to the core-shell-like structure formation, but is essential for preserving the crystallinity of

the sample (Figure 1). Note that the leaching in the sole presence of oxalic acid indeed results in a substantial loss of crystallinity (Figure 1) without any core-shell hierarchical zeolite formation (Figure 2a).

We further emphasize on the single-crystal architecture and the excellent interconnectivity between the core and shell of the zeolite samples reported here. While many core-shell zeolites have been synthesized [42, 44-49], a zeolite with well interconnected micro- and/or meso-porous core and a rough mesoporous shell is rare [28, 42, 50]. Core-shell boundary and misaligned shell growth are some of the undesired consequences of many previously reported techniques applied for the preparation of core-shell materials. The interfaces between the core and shell may constitute diffusion boundaries due to possible mismatching in the alignment of different microporous domains [51]. In our case, the shell is created by the intensive dissolution of the outermost shell of the same crystals. It can, therefore, be expected that the continuous channels with mesoporous openings will permit unhindered access guest molecules to diffuse in the intrinsic 3D porous network of zeolites.

3.3 Tuning the core-shell structure

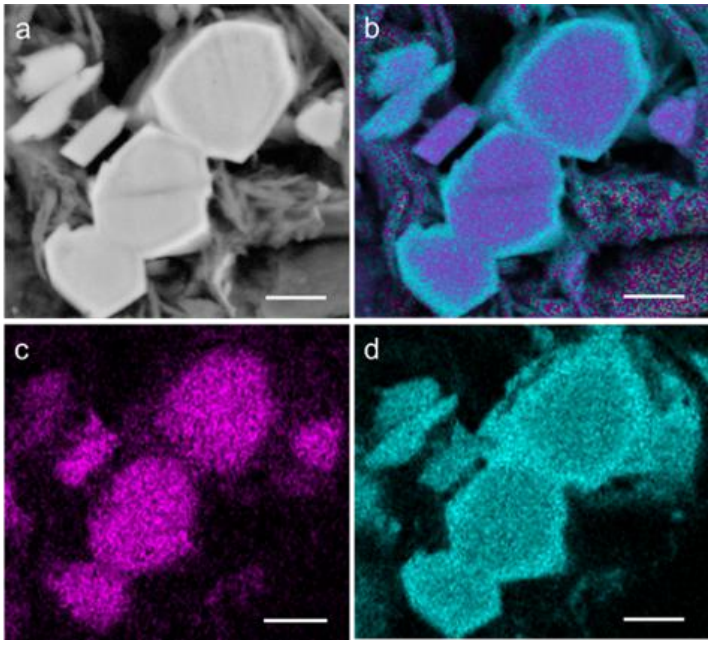

Figure 7. SEM EDX mapping of AFY2 zeolite (a: SEM image, b: EDX mapping image of overlapping Al with Si, c: EDX mapping image of Al, d: EDX mapping

image of Si), scale bar = 1 μm.

The structure of the core-shell-like hierarchical zeolite can be further tailored by adjusting the treatment conditions, such as the concentration of the active species. The concentration of oxalic acid was decreased by 40% in the mixture of OA-NH_4F (experimental part) and used for treatment of the parent zeolite (PY). The AFY2 sample also exhibits a similar rough surface morphology as the AFY1 (Figures S2 and S7). The core-shell-like characteristic of this sample was further confirmed by advanced SEM characterization showing the enrichment of mesopores in the crystals periphery (Figure S8). The EDX mapping of the AFY2 shows a distinct core-shell morphology with a Si-rich shell (Figure 7). In line with this data, the surface Si/Al as determined by XPS is 11.7, and the bulk Si/Al is 4.0. These results confirmed that that the intensive surface etching is controlled by the overall ion strength of the active fluoride species (both Si and Al active), but not by the concentration of oxalic acid along. Noting that the AY sample treated by the oxalic acid has the same smooth surface as the PY (Figure S3a). On the other hand, both the surface and bulk Si/Al ratios of sample AFY2 are lower than that of AFY1. AFY2 also shows higher microporosity (+0.08 $cm^3\ g^{-1}$, Table 1) and a measurable increase in the crystallinity (Figure 1) without losing the hierarchical core-shell-like characteristics. A careful comparison of the EDX mapping indicates that the acid etching depth decreased in the case of AFY2 (Figures 6 and 7). This is a clear sign that the concentration of oxalic acid has an impact on the microporosity of the samples, their chemical composition and on the thickness of the Si-rich shell of zeolite crystals.

3.4 Tuning the zeolite surface: turning trade-offs into synergies

We believe that the mixture OA-NH_4F works as a bifunctional reagent during the chemical etching process. Namely, NH_4F and more specifically its fluoride derivatives are responsible for framework demetallation (simultaneous Si and Al removal), while the oxalic acid is responsible for the additional framework dealumination. The OA-NH_4F etching is a diffusion-controlled process, and the intrinsic activity of the NH_4F-oxalic acid etchant is expected to be very high. This can be rationalized by

considering that the dissolution of zeolite crystals should be more homogeneous over space and time, if the dissolution is a kinetically controlled process [34]. Because of the different kinetics between surface dissolution and intra particle transport of etchants, extensive etching of zeolite was limited on crystal surface. This facilitates the permeation of the chelating agent and favors surface layer dealumination. As a supporting argument, both AFY1 and AFY2 zeolites show higher bulk Si/Al ratios than their oxalic acid treated counterparts (5.5 *vs* 5.4 and 4.0 *vs* 3.7, respectively). The Si/Al surface ratios of AFY1 (14.3) and AFY2 (11.7) are also higher than that of AY (11.4). Noting that the concentration of oxalic acid used for AY treatment is equal to that used for AFY1 and 1.6 times more than what used for AFY2. Additional argument comes from the molecular simulation results, which showed that the aluminum trioxalate complex has a longest dimension of 0.64 nm [36]. Although this is barely smaller than the pore opening of FAU, the countercurrent diffusion of dissolved aluminum trioxalate coming out should compete with other incoming etchant species and solvent molecules for micropore space. Thus, the chemical etching process itself serves as the first evidence that the "digging" of crystal surface has successfully turned the underperforming surface wall into a high permeable shell. This may facilitate the contact between Al in zeolite framework and the oxalic acid chelating agent.

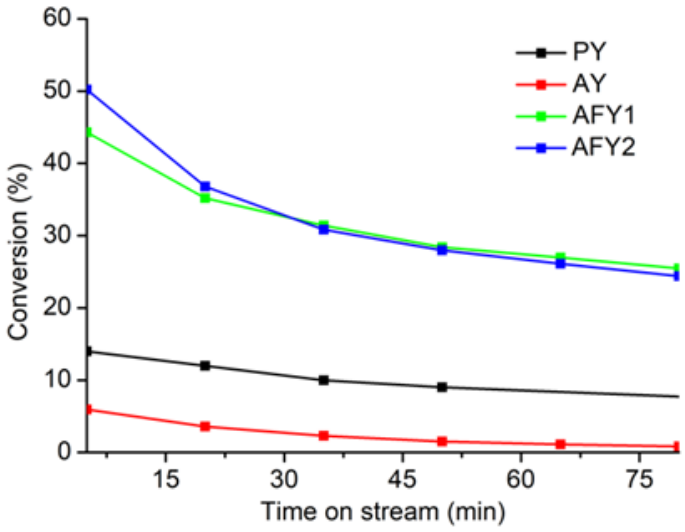

Figure 8. Dealkylation of 1,3,5-triisopropylbenzene on PY (parent zeolite Y), AY (oxalic acid treated zeolite Y) and hierarchical core-shell-like zeolites AFY1 and AFY2 (oxalic acid and NH_4F. Reaction conditions: T = 498 K, W/F_0 = 0.022 kg h mol^{-1}, P = 0.1 MPa.

As a second example highlighting the improved permeability of the zeolite periphery (shell), the dealkylation of 1,3,5-triisopropylbenzene (TiPBz) as a model reaction was carried out (Figure 8). The bulky TiPBz is known to probe specifically the external or mesoporous surfaces of zeolites [34, 52]. As expected, TiPBz conversion is lower on the parent zeolite PY but increases significantly for the AFY1. The surface Si/Al ratio of sample AFY1 is 14.3, while the Si/Al ratio of PY is 2.6, which unambiguously demonstrates that the accessibility of the inner structure of sample AFY1 is substantially improved. Noticeably, AFY2 showed higher initial activity for dealkylation of TiPBz than AFY1, which corresponds to the higher crystallinity (Figure 1) and acidity of the former core-shell-like structure (Table 1, Figure S6). Apparently, higher crystallinity (hence higher acidity) in the porous shell is responsible for the higher initial activity of the AFY2 zeolite. AY showed lower TiPBz conversion with time-on-stream than PY. The lower conversion is attributed to the substantially decreased surface active sites and poor surface permeability.

4. Conclusion

In conclusion, we have developed a simple top-down approach for the preparation of core-shell-like zeolites. This was achieved by diffusion-controlled chemical etching of zeolite crystals with oxalic acid and NH_4F mixed solution (OA-NH_4F). The fast dissolution kinetics and the relatively slower intra-crystalline diffusion of the solutions limited the intensive dissolution of zeolite crystals only at the periphery. OA-NH_4F served as a bifunctional etchant, extracted both surface Si and Al, and further caused dealumination. This resulted in a distinct core-shell-like structure with a rough, porous, and Si-rich shell. Such a hierarchical core-shell-like zeolite is analogous to a bottom-up core-shell zeolite but with the unique advantages of preserving the single crystals characteristic, completely interconnected micro- and

mesopores and rough mesoporous surface. The core-shell-like zeolites can serve as a model system for surface permeability and diffusion studies, and to evaluate the effect of Al gradient on the catalytic performance due to the Si-rich shell.

Conflicts of interest

The authors declare no competing financial interest.

Acknowledgements

The authors acknowledge funding from the Sino-French joint laboratory "Zeolites", and the funding from NSFC (21978326, 21706285, 21975285 21991090 and 21991091), Qingdao Applied Basic Research Project (19-6-2-70-cg), the Fundamental Research Funds for the Central Universities (18CX02013A), and the Natural Science Foundation of Shandong Province (ZR2019MB029). S.M. acknowledges the support from Thousand Talents Program for Foreign Experts (WQ20152100316). The authors thank Desheng Xi from JEOL for his support on the preparation of cross-sections and SEM-EDX mappings of the samples.

References

1. W. Vermeiren, J-P. Gilson, Impact of zeolites on the petroleum and petrochemical industry, Topics in Catalysis, 2009, 52(9): 1131-1161.
2. C. Martínez, A. Corma, Inorganic molecular sieves: Preparation, modification and industrial application in catalytic processes, Coordination Chemistry Reviews, 255 (2011) 1558-1580.
3. S. Mintova, N. Olson, V. Valtchev, T. Bein, Mechanism of zeolite A nanocrystal growth from colloids at room temperature, Science, 1999, 283(5404): 958-960.
4. A. Corma, M. Díaz-Cabañas, J. Jordá, C. Martínez, M. Moliner, High-throughput synthesis and catalytic properties of a molecular sieve with 18-and 10-member rings, Nature, 2006, 443(7113): 842-845.
5. J. Pérez-Ramírez, C. Christensen, K. Egeblad, et al. Hierarchical zeolites:

enhanced utilisation of microporous crystals in catalysis by advances in materials design[J]. Chemical Society Reviews, 2008, 37(11): 2530-2542.

6. L.-H. Chen, M.-H. Sun, Z. Wang, W. Yang, Z. Xie, B.-L. Su, Hierarchically Structured Zeolites: From Design to Application, Chemical Reviews, 2020, 120(20): 11194-11294.

7. T. Ohsuna, O. Terasaki, D. Watanabe, M.W. Anderson, S.W. Carr, Dealumination of hexagonal (EMT)/cubic (FAU) zeolite intergrowth materials: A SEM and HRTEM study, Chemistry of materials, 6 (1994) 2201-2204.

8. Z. Qin, B. Shen, X. Gao, F. Lin, B. Wang, C. Xu, Mesoporous Y zeolite with homogeneous aluminum distribution obtained by sequential desilication–dealumination and its performance in the catalytic cracking of cumene and 1, 3, 5-triisopropylbenzene, Journal of catalysis, 278 (2011) 266-275.

9. D. Yuan, C. Kang, W. Wang, H. Li, X. Zhu, Y. Wang, X. Gao, B. Wang, H. Zhao, C. Liu, B. Shen, Creation of mesostructured hollow Y zeolite by selective demetallation of an artificial heterogeneous Al distributed zeolite crystal, Catalysis Science & Technology, 6 (2016) 8364-8374.

10. C. Li, L. Guo, P. Liu, K. Gong, W. Jin, L. Li, X. Zhu, X. Liu, B. Shen, Defects in AHFS-dealuminated Y zeolite: A crucial factor for mesopores formation in the following base treatment procedure, Microporous and mesoporous materials, 255 (2018) 242-252.

11. Z. Qin, L. Pinard, M.A. Benghalem, T.J. Daou, G. Melinte, O. Ersen, S. Asahina, J.-P. Gilson, V. Valtchev, Preparation of Single Crystals “House-of-Cards”-like ZSM-5 and Their Performance in Ethanol-to-Hydrocarbons Conversion, Chemistry of Materials, 31 (2019) 4639-4648.

12. J.C. Groen, T. Bach, U. Ziese, A.M. Paulaime-van Donk, K.P. De Jong, J.A. Moulijn, J. Pérez-Ramírez, Creation of hollow zeolite architectures by controlled

desilication of Al-zoned ZSM-5 crystals, Journal of the American Chemical Society, 127 (2005) 10792-10793.

13. C. Mei, Z. Liu, P. Wen, Z. Xie, W. Hua, Z. Gao, Regular HZSM-5 microboxes prepared via a mild alkaline treatment, Journal of Materials Chemistry, 18 (2008) 3496-3500.

14. Y. Wang, A. Tuel, Nanoporous zeolite single crystals: ZSM-5 nanoboxes with uniform intracrystalline hollow structures, Microporous and Mesoporous Materials, 113 (2008) 286-295.

15. C. Dai, A. Zhang, L. Li, K. Hou, F. Ding, J. Li, D. Mu, C. Song, M. Liu, X. Guo, Synthesis of hollow nanocubes and macroporous monoliths of silicalite-1 by alkaline treatment, Chemistry of Materials, 25 (2013) 4197-4205.

16. C. Xia, M. Lin, B. Zhu, Y. Luo, X. Shu, Hollow Titanium Silicalite Zeolite: From Fundamental Research to Commercial Application in Environmental-Friendly Catalytic Oxidation Processes, Zeolites: Useful Minerals, (2016) 109.

17. R. Dessau, E. Valyocsik, N. Goeke, Aluminum zoning in ZSM-5 as revealed by selective silica removal, Zeolites, 12 (1992) 776-779.

18. M.W. Anderson, J.R. Agger, J.T. Thornton, N. Forsyth, Crystal Growth in Zeolite Y Revealed by Atomic Force Microscopy, Angewandte Chemie, 35 (1996) 1210-1213.

19. P. Cubillas, S.M. Stevens, N. Blake, A. Umemura, C.B. Chong, O. Terasaki, M.W. Anderson, AFM and HRSEM Invesitigation of Zeolite A Crystal Growth. Part 1: In the Absence of Organic Additives, Journal of Physical Chemistry C, 115 (2011) 12567-12574.

20. J.R. Agger, N. Hanif, C.S. Cundy, A.P. Wade, S. Dennison, P.A. Rawlinson, M.W. Anderson, Silicalite Crystal Growth Investigated by Atomic Force Microscopy, Journal of the American Chemical Society, 125 (2003) 830-839.

21. J.E. Schmidt, F.C. Hendriks, M. Lutz, L.C. Post, D. Fu, B.M. Weckhuysen,

Diagnosing the Internal Architecture of Zeolite Ferrierite, ChemPhysChem, 19 (2018) 367-372.

22. Y. Shen, S. Asahina, N. Asano, G. Zhang, S. Qian, Y. Ma, Z.-F. Yan, X. Liu, S. Mintova, The inner heterogeneity of ZSM-5 zeolite crystals, Journal of Materials Chemistry A, (2021). (DOI: 10.1039/D0TA11023J)

23. J. Kaerger, In-depth study of surface resistances in nanoporous materials by microscopic diffusion measurement, Microporous and mesoporous materials, 189 (2014) 126-135.

24. J. Zhou, W. Fan, Y. Wang, Z. Xie, The essential mass transfer step in hierarchical/nano zeolite: surface diffusion, National Science Review, 7(11) (2020) 1630-1632.

25. S.J. Reitmeier, O.C. Gobin, A. Jentys, J.A. Lercher, Enhancement of Sorption Processes in the Zeolite H- ZSM5 by Postsynthetic Surface Modification, Angewandte Chemie International Edition, 48 (2009) 533-538.

26. A. Guerrero-Martinez, J. Perez-Juste, L.M. Liz-Marzan, Recent Progress on Silica Coating of Nanoparticles and Related Nanomaterials, Advanced Materials, 22 (2010) 1182-1195.

27. M. Enterria, F. Suarez-Garcia, A. Martinez-Alonso, J.M.D. Tascon, Preparation of hierarchical micro-mesoporous aluminosilicate composites by simple Y zeolite/MCM-48 silica assembly, Journal of Alloys and Compounds, 583 (2014) 60-69.

28. X. Qian, J. Du, B. Li, M. Si, Y. Yang, Y. Hu, G. Niu, Y. Zhang, H. Xu, B. Tu, Y. Tang, D. Zhao, Controllable fabrication of uniform core–shell structured zeolite@ SBA-15 composites, Chemical Science, 2 (2011) 2006-2016.

29. D. Zhao, J. Sun, Q. Li, G.D. Stucky, Morphological control of highly ordered mesoporous silica SBA-15, Chemistry of materials, 12 (2000) 275-279.

30. J. Vartuli, K. Schmitt, C. Kresge, W. Roth, M. Leonowicz, S. McCullen, S.

Hellring, J. Beck, J. Schlenker, D. Olson, E. Sheppard, Effect of surfactant/silica molar ratios on the formation of mesoporous molecular sieves: inorganic mimicry of surfactant liquid-crystal phases and mechanistic implications, Chemistry of materials, 6 (1994) 2317-2326.

31. X. Qian, B. Li, Y. Hu, G. Niu, D. Zhang, R. Che, Y. Tang, D. Su, M. Asiri, D. Zhao, Exploring Meso-/Microporous Composite Molecular Sieves with Core-Shell Structures, Chemistry-a European Journal, 18 (2012) 931-939.

32. Z. Qin, G. Melinte, J.P. Gilson, M. Jaber, K. Bozhilov, P. Boullay, S. Mintova, O. Ersen, V. Valtchev, The mosaic structure of zeolite crystals, Angewandte Chemie International Edition, 55 (2016) 15049-15052.

33. Z. Qin, L. Lakiss, J.-P. Gilson, K. Thomas, J.-M. Goupil, C. Fernandez, V. Valtchev, Chemical equilibrium controlled etching of MFI-type zeolite and its influence on zeolite structure, acidity, and catalytic activity, Chemistry of Materials, 25 (2013) 2759-2766.

34. Z. Qin, K.A. Cychosz, G. Melinte, H. El Siblani, J.-P. Gilson, M. Thommes, C. Fernandez, S. Mintova, O. Ersen, V. Valtchev, Opening the cages of Faujasite-type zeolite, Journal of the American Chemical Society, 139 (2017) 17273-17276.

35. Z. Qin, L. Hafiz, Y. Shen, S. Van Daele, P. Boullay, V. Ruaux, S. Mintova, J.-P. Gilson, V. Valtchev, Defect-engineered zeolite porosity and accessibility, Journal Of Materials Chemistry A, 8 (2020) 3621-3631.

36. M.R. Apelian, A.S. Fung, G.J. Kennedy, T.F. Degnan, Dealumination of zeolite β via dicarboxylic acid treatment, The Journal of Physical Chemistry, 100 (1996) 16577-16583.

37. Z. Yan, D. Ma, J. Zhuang, X. Liu, X. Liu, X. Han, X. Bao, F. Chang, L. Xu, Z. Liu, On the acid-dealumination of USY zeolite: a solid state NMR investigation, Journal of Molecular Catalysis A: Chemical, 194 (2003) 153-167.

38. M. Thommes, K. Kaneko, A.V. Neimark, J.P. Olivier, F. Rodriguez-Reinoso, J. Rouquerol, K.S. Sing, Physisorption of gases, with special reference to the evaluation of surface area and pore size distribution (IUPAC Technical Report), Pure and Applied Chemistry, 87 (2015) 1051-1069.

39. T. Yokoi, Characterization of zeolites by advanced SEM/STEM techniques, HITACHI Tokyo, Japan:2016.

40. T. Prasomsri, W. Jiao, S.Z. Weng, J.G. Martinez, Mesostructured zeolites: bridging the gap between zeolites and MCM-41, Chemical Communications, 51 (2015) 8900-8911.

41. T. Li, J. Ihli, J.T. Wennmacher, F. Krumeich, J.A. van Bokhoven, The Link between ZSM- 5 Zeolite Crystallization and Mesopore Formation by Leaching, Chemistry–A European Journal, 25 (2019) 7689-7694.

42. Y. Bouizi, I. Diaz, L. Rouleau, V.P. Valtchev, Core–shell zeolite microcomposites, Advanced Functional Materials, 15 (2005) 1955-1960.

43. Z. Qin, J.-P. Gilson, V. Valtchev, Mesoporous zeolites by fluoride etching, Current Opinion in Chemical Engineering, 8 (2015) 1-6.

44. D. Mochizuki, R. Sasaki, M.M. Maitani, M. Okamoto, E. Suzuki, Y. Wada, Catalytic reactions enhanced under microwave-induced local thermal non-equilibrium in a core–shell, carbon-filled zeolite@ zeolite, Journal of catalysis, 323 (2015) 1-9.

45. Y. Bouizi, L. Rouleau, V.P. Valtchev, Factors controlling the formation of core− shell zeolite− zeolite composites, Chemistry of materials, 18 (2006) 4959-4966.

46. A. Ghorbanpour, A. Gumidyala, L.C. Grabow, S.P. Crossley, J.D. Rimer, Epitaxial growth of ZSM-5@ Silicalite-1: A core–shell zeolite designed with passivated surface acidity, ACS nano, 9 (2015) 4006-4016.

47. Y. Bouizi, G. Majano, S. Mintova, V. Valtchev, Beads comprising a hierarchical porous core and a microporous shell, Journal Of Physical Chemistry C, 111

(2007) 4535-4542.

48. G.D. Pirngruber, C. Laroche, M. Maricar-Pichon, L. Rouleau, Y. Bouizi, V. Valtchev, Core–shell zeolite composite with enhanced selectivity for the separation of branched paraffin isomers, Microporous and mesoporous materials, 169 (2013) 212-217.

49. Z. Jin, S. Liu, L. Qin, Z. Liu, Y. Wang, Z. Xie, X. Wang, Methane dehydroaromatization by Mo-supported MFI-type zeolite with core–shell structure, Applied Catalysis A: General, 453 (2013) 295-301.

50. J.-S. Yu, S.B. Yoon, Y.J. Lee, K.B. Yoon, Fabrication of bimodal porous silicate with silicalite-1 core/mesoporous shell structures and synthesis of nonspherical carbon and silica nanocases with hollow core/mesoporous shell structures, The Journal of Physical Chemistry B, 109 (2005) 7040-7045.

51. L. Karwacki, M.H. Kox, D.M. De Winter, M.R. Drury, J.D. Meeldijk, E. Stavitski, W. Schmidt, M. Mertens, P. Cubillas, N. John, Morphology-dependent zeolite intergrowth structures leading to distinct internal and outer-surface molecular diffusion barriers, Nature materials, 8 (2009) 959-965.

52. H. Awala, J.-P. Gilson, R. Retoux, P. Boullay, J.-M. Goupil, V. Valtchev, S. Mintova, Template-free nanosized faujasite-type zeolites, Nature materials, 14 (2015) 447-451.